ORGANOMETALLICS

Article

pubs.acs.org/Organometallics

Hidden Enantioselective Hydrogenation of N-Silyl Enamines and Silyl Enol Ethers in Net C═N and C═O Hydrosilylations Catalyzed by Ru−S Complexes with One Monodentate Chiral Phosphine Ligand

Susanne Bähr and Martin Oestreich*

Institut für Chemie, Technische Universität Berlin, Strasse des 17. Juni 115, 10623 Berlin, Germany

Supporting Information

ABSTRACT: Ruthenium thiolate complexes with one chiral monodentate phosphine ligand are applied to enantioselective hydrosilylation of enolizable imines and ketones. The structural features of the catalyst exclude the presence of more than one phosphine ligand at the ruthenium center in the enantioselectivity-determining step. The enantiomeric excesses obtained in these reduction reactions are moderate (up to 66% ee), but the stereochemical outcome enables an experimental analysis of the reaction pathways operative in this catalysis. A two-step sequence consisting of successive N−Si/O−Si dehydrogenative coupling and enamine/enol ether hydrogenation is the prevailing mechanism of action. Both steps involve cooperative bond activation at the Ru−S bond of the coordinatively unsaturated ruthenium complex: Si−H bond activation in the dehydrogenative coupling and heterolytic H−H splitting in the hydrogenation. Previously documented side reactions such as deprotonation/protonation equilibria as well as competing direct C═N or C═O hydrogenation have been excluded.

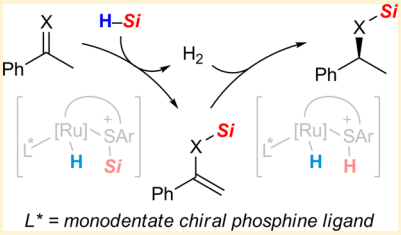

INTRODUCTION

A few years ago, Ohki and Tatsumi reported the synthesis of the ruthenium(II) thiolate complexes $[\mathbf{1}]^+[BAr^F{}_4]^-$ (Scheme 1, top left) and their application in the catalytic hydrogenation of carbonyl compounds.[1] The cooperative bond activation of hydrosilanes with $[\mathbf{1}]^+[BAr^F{}_4]^-$ was later investigated in great detail, revealing the formation of a ruthenium hydride together with a sulfur-stabilized silylium ion ($[\mathbf{1}]^+ \rightarrow [\mathbf{2}]^+$; Scheme 1, top right).[2] In collaboration with Ohki and Tatsumi, our group was also able to catalytically access the electrophilic silicon species $[\mathbf{2}]^+$, and several transformations including electrophilic C−H silylations[3] or hydrodefluorinations[4] were accomplished. A few of those catalytic reactions result in the formation of chiral compounds such as benzosiloles[5] and 4-substituted 1,4-dihydropyridines[6] (Scheme 1, bottom). These latter examples are of particular interest, as enantioenriched silicon-stereogenic benzosiloles are rare,[7] and the enantioselective synthesis of N-silylated 1,4-dihydropyridines is even unprecedented. Conversely, the asymmetric hydrosilylation of ketones[8] and ketimines[9] can be regarded as a solved problem.[10] Especially the former of these two transformations serves as a benchmark reaction for the purpose of evaluating the performance of new chiral catalysts. To make chiral congeners of $[\mathbf{1}]^+[BAr^F{}_4]^-$, we considered several approaches to introduce chirality, one being the replacement of the ligand L in $[\mathbf{1}]^+[BAr^F{}_4]^-$ by a chiral monodentate phosphorus ligand L*.[11]

However, several structural and electronic requirements must be fulfilled to obtain catalytically active complexes. (1) The vacant coordination site at ruthenium must be retained. This a priori excludes bidentate ligands, e.g., binap, or ligands with additional Lewis basic groups. (2) Steric bulk around and electronic properties of the phosphorus atom are restricted. Sterically demanding as well as electron-deficient ligands have been shown not to be compatible with the electron-deficient ruthenium center in Ohki−Tatsumi complexes.[12] To us,

Scheme 1. Potential Applications of $[\mathbf{1}]^+[BAr^F{}_4]^-$ in Asymmetric Catalysis[a]

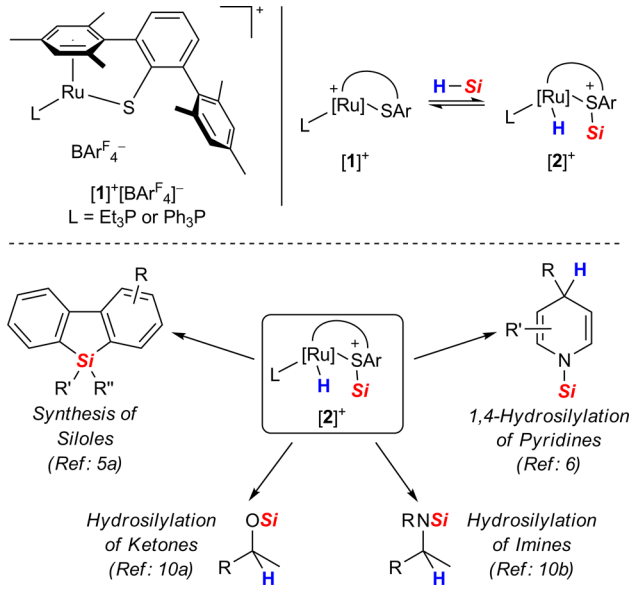

[a] Ar^F = 3,5-bis(trifluoromethyl)phenyl.

Received: January 12, 2017

DOI: 10.1021/acs.organomet.7b00030
Organometallics XXXX, XXX, XXX−XXX

monodentate phosphines appeared appropriate for the preparation of chiral variants of $[\mathbf{1}]^+[BAr^F{}_4]^-$.[13] Chiral phosphines **3** with an asymmetrically substituted phosphorus atom represent one class of such potentially suitable ligands (Chart 1, top). **3** was initially applied in asymmetric

Chart 1. Monodentate Chiral Phosphine Ligands

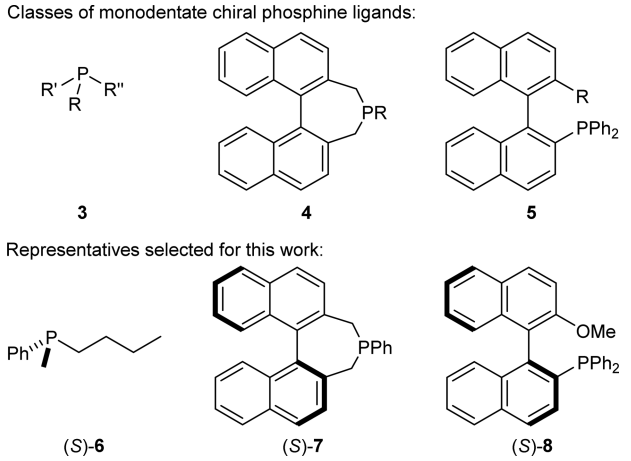

hydrogenation[14] and hydrosilylation[15] with success, and further applications with different metals are known today.[13a,c,16] As another ligand class, binol-derived phosphepines **4** introduced by Gladiali[17] and then further elaborated by Beller[18] are attractive. Apart from hydrogenation reactions,[18a,b] compounds **4** were also applied in enantioselective carbonyl hydrosilylation.[19] It is important to note though that, for application of both **3** and **4**, two ligand molecules are coordinating the metal center during the catalysis, and the use of only 1 equiv of the chiral phosphine on the basis of catalyst loading was shown to be detrimental for both conversion and enantioinduction.[20] The situation changes with Hayashi's phosphines **5**.[13b,21] These were especially designed for those cases where bidentate, chelating phosphine ligands such as binap lead to less active catalysts.[22]

We hence envisioned the synthesis of chiral ruthenium thiolate complexes with just one monodentate chiral phosphine as the origin of enantioinduction. One congener each of the above ligands ((*S*)-**6**−(*S*)-**8**; Chart 1, bottom) was chosen to replace the achiral phosphine ligand in $[\mathbf{1}]^+[BAr^F{}_4]^-$. The new complexes have been applied as catalysts in the enantioselective net hydrosilylation of C═N and C═O bonds involving cooperative Si−H bond activation.[23] The reaction is found to follow a sequence of dehydrogenative N−Si or O−Si coupling and hydrogenation of the intermediate N-silyl enamines and silyl enol ethers, respectively.

RESULTS AND DISCUSSION

Our investigations on chiral ruthenium(II) thiolate complexes started with the synthesis of monodentate phosphine ligands. We decided to use one typical representative of each class (Chart 1, bottom). (*S*)-**6** described by Genêt and Jugé,[24] phosphepine (*S*)-**7**,[18a,b] and (*S*)-**8**[21] were synthesized according to reported procedures. The targeted catalyst precursors ($R,^{Ru}RS$)-**9**, ($S,^{Ru}RS$)-**10**, and ($S,^{Ru}RS$)-**11** (Table 1) were tackled following the established protocol for the preparation of the achiral ruthenium chlorides. The indicated chiral phosphine ligand was added to in situ prepared[4,10b] or isolated[1] ruthenium

Table 1. Synthesis of Chiral Ruthenium Chloride Complexes

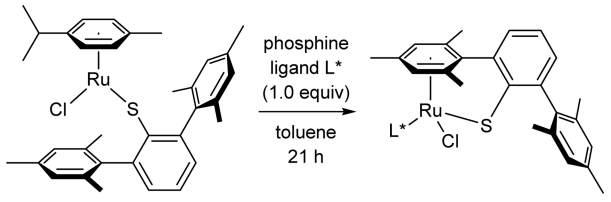

entry	L*	*T* (°C)	complex	yield (%)[a]	dr[b]
1	(*S*)-**6**	65	($R,^{Ru}RS$)-**9**	45	52:48
2	(*S*)-**7**	80	($S,^{Ru}RS$)-**10**	71	82:18
3	(*S*)-**8**	65	($S,^{Ru}RS$)-**11**	0	

[a]Isolated yields after flash column chromatography. [b]Diastereomeric ratio determined by ^{1}H NMR spectroscopy.

complex **12** in toluene. ($R,^{Ru}RS$)-**9** and ($S,^{Ru}RS$)-**10** were isolated in moderate and good yields, respectively, as a mixture of two diastereomers (entries 1 and 2). However, coordination of (*S*)-**8** to the ruthenium center in **12** was not observed, and the corresponding chloride complex ($S,^{Ru}RS$)-**11** was not obtained (entry 3). We ascribe this to the steric demand of ligand (*S*)-**8**.

For the other two complexes, we noticed the predominant formation of one diastereomer, especially in the case of phosphepine (*S*)-**7** as the ligand (forming ($S,^{Ru}RS$)-**10**). The major diastereomer ($S,^{Ru}R$)-**10** is obtained exclusively by crystallization, as revealed by ^{1}H NMR analysis of the crystalline solid (Scheme 2, bottom). Another ^{1}H NMR

Scheme 2. Configurational Instability of the Ruthenium Center

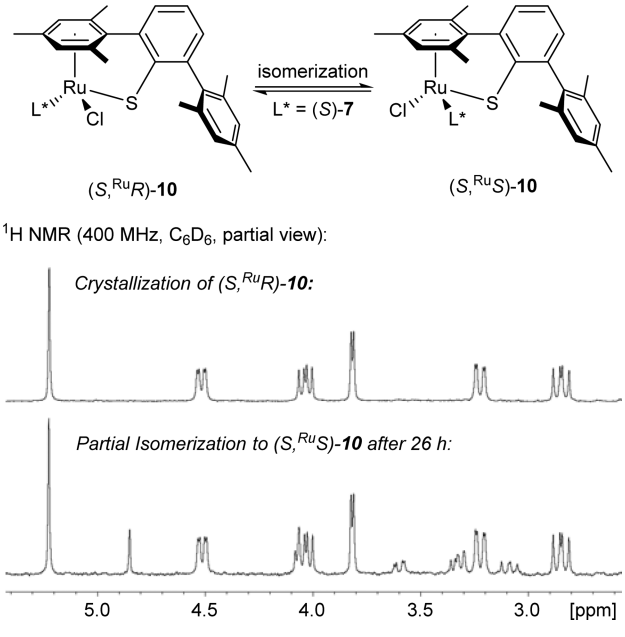

measurement of the same sample after 1 day showed that epimerization at ruthenium of ($S,^{Ru}R$)-**10** occurred in solution. The originally obtained dr of 82:18 was reestablished (for a full ^{1}H NMR spectrum, see the Supporting Information).

It was further possible to secure the molecular structure of the major diastereomer ($S,^{Ru}R$)-**10** by X-ray diffraction analysis

DOI: 10.1021/acs.organomet.7b00030
Organometallics XXXX, XXX, XXX−XXX

(Scheme 3, left).[25] The configurational lability of the ruthenium center in the chloride complexes is irrelevant in subsequent steps, as this stereoinformation is lost in the following chloride abstraction. Treatment of (S,^{Ru}RS)-**10** with $NaBAr^F_4$ results in the formation of cationic complex $[(S)\text{-}\mathbf{13}]^+[BAr^F_4]^-$ ((S,^{Ru}RS)-**10** → $[(S)\text{-}\mathbf{13}]^+[BAr^F_4]^-$; Scheme 3, right). $[(S)\text{-}\mathbf{13}]^+[BAr^F_4]^-$ was isolated in 70% yield.

Scheme 3. Structure of (S,^{Ru}R)-10[a] and Synthesis of $[(S)\text{-}\mathbf{13}]^+[BAr^F_4]^-$

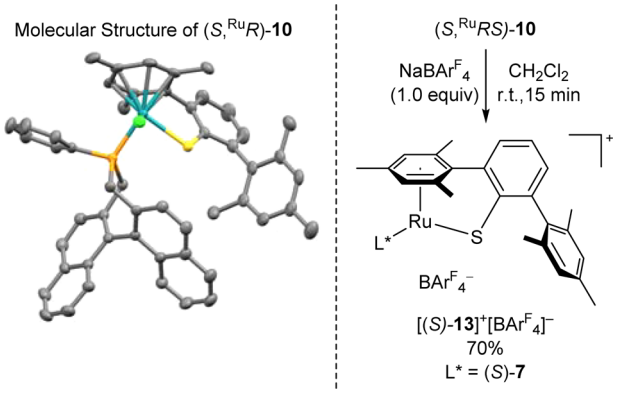

[a]Thermal ellipsoids represent the 50% probability level. Hydrogen atoms and solvent molecules have been removed for the sake of clarity.

With the ruthenium complexes in hand, we began testing their potential in enantioselective hydrosilylation. We used 1 mol % of either chloride (S,^{Ru}RS)-**9** and (R,^{Ru}RS)-**10** together with $NaBAr^F_4$ for the in situ generation of the active catalysts. These were then combined with Me_2PhSiH and phenyl-protected imine **14** (Table 2). The corresponding amine **15** was isolated after hydrolysis of the N–Si bond (**14** → **16** → **15**), but in the case of (R,^{Ru}RS)-**9** it was obtained in a low yield of 20% and as a racemate (entry 1). (S,^{Ru}RS)-**10** together with $NaBAr^F_4$ resulted not only in near-quantitative yield but also in promising 53% ee, with (S)-**15** being the major enantiomer (entry 2). Preformed chloride-free $[(S)\text{-}\mathbf{13}]^+[BAr^F_4]^-$ furnished the same enantioselectivity (entry 3),[26] thereby making interference by chloride-bridged dimers[4] unlikely.[27] It turned out that the level of enantiocontrol did not vary at different conversions; (S)-**15** was obtained after 0.5 and 1 h in diminished yields of 48% and 61% with the enantiomeric excess unchanged (entries 3 and 4). Furthermore, considerable amounts of enamine **17** were detected by NMR spectroscopy when the reaction was stopped after 0.5 h (see the Supporting Information), whereas **17** was almost completely reduced to the amine (S)-**16** after 3 h (entry 5). N- and C2-disilylated **18** which would result from 2-fold dehydrogenative coupling was not observed.[28] The substitution pattern on the silicon atom had little effect on the enantioinduction: $MePh_2SiH$, Et_3SiH, and Me_2EtSiH reacted with selectivities similar to that of Me_2PhSiH (entries 6–8). However, a high yield was obtained with $MePh_2SiH$. With Ph_3SiH (entry 9), both the enantiomeric excess and yield dropped significantly. $PhSiH_3$ resulted in full conversion but hardly any enantioinduction (entry 10). In addition, surrogate **19**[29] was suitable for the catalysis with $[(S)\text{-}\mathbf{13}]^+[BAr^F_4]^-$ under the same setup and resulted again in 53% ee (see the box in the graphic of Table 2). This result shows that cyclohexa-1,4-diene-based surrogate **19** can be activated by $[(S)\text{-}\mathbf{13}]^+[BAr^F_4]^-$,[30] thereby engaging in enantioselective transfer hydrosilylation using chiral Ohki–Tatsumi complexes.

A similar screening was performed with acetophenone (**20**) in combination with catalyst $[(S)\text{-}\mathbf{13}]^+[BAr^F_4]^-$ (Table 3). With hydrosilane Me_2PhSiH, an even better 65% ee was obtained for silyl ether (S)-**21a**; the corresponding silyl enol ether **22**[10a] was not isolated in this particular reaction (entry 1).

Table 2. Hydrosilylation of Imine 14[a]

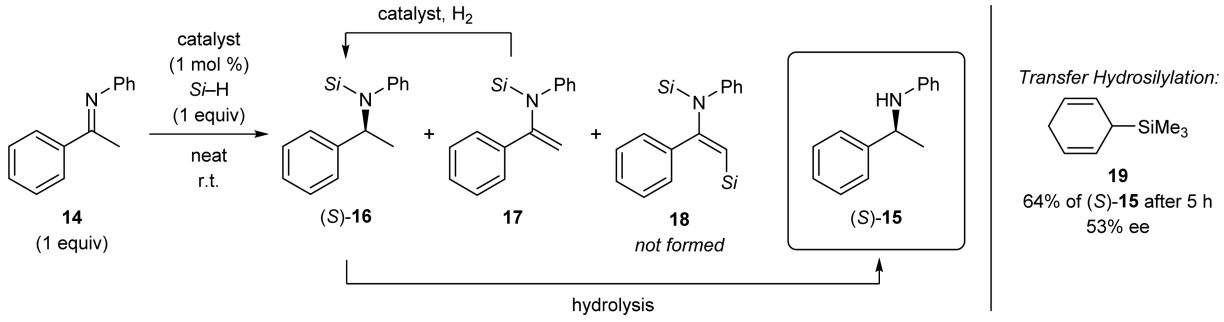

entry	catalyst system	*Si*–H	time (h)	yield of (S)-**15**[b] (%)	ee[c] (%)
1	(R,^{Ru}RS)-**9**/$NaBAr^F_4$	Me_2PhSiH	22	20	0
2	(S,^{Ru}RS)-**10**/$NaBAr^F_4$	Me_2PhSiH	22	99	53
3	$[(S)\text{-}\mathbf{13}]^+[BAr^F_4]^-$	Me_2PhSiH	0.5	48	54
4	$[(S)\text{-}\mathbf{13}]^+[BAr^F_4]^-$	Me_2PhSiH	1	61	53
5	$[(S)\text{-}\mathbf{13}]^+[BAr^F_4]^-$	Me_2PhSiH	3	96	54
6	$[(S)\text{-}\mathbf{13}]^+[BAr^F_4]^-$	$MePh_2SiH$	3	93	53
7	$[(S)\text{-}\mathbf{13}]^+[BAr^F_4]^-$	Et_3SiH	3	61	54
8	$[(S)\text{-}\mathbf{13}]^+[BAr^F_4]^-$	Me_2EtSiH	3	71	55
9[d]	$[(S)\text{-}\mathbf{13}]^+[BAr^F_4]^-$	Ph_3SiH	3	35	36
10	$[(S)\text{-}\mathbf{13}]^+[BAr^F_4]^-$	$PhSiH_3$	3	99	<5[e]

[a]All reactions were performed according to GP1 (see the Experimental Section) on a 0.2 mmol scale. [b]Isolated yield after flash column chromatography. [c]Determined with HPLC on a chiral stationary phase. [d]Performed with C_6H_6 (0.1 mL) as solvent. [e](R)-**15** was obtained as major enantiomer.

DOI: 10.1021/acs.organomet.7b00030
Organometallics XXXX, XXX, XXX–XXX

Table 3. Hydrosilylation of Ketone 20[a,b]

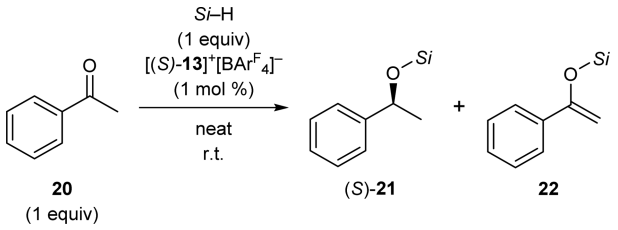

entry	Si–H	time (h)	silyl ether	yield (%)[c]	ee (%)[d]	(S)-21:22[e]
1	Me_2PhSiH	2	(S)-**21a**	93	65	100:0
2	Me_2PhSiH	1.5	(S)-**21a**	nd	66	91:9
3	Me_2PhSiH	1	(S)-**21a**	nd	66	68:32
4	$MePh_2SiH$	3	(S)-**21b**	82[f]	66	100:0
5	Et_3SiH	3	(S)-**21c**	82	51	100:0

[a]All reactions were performed according to GP2 (see the Experimental Section) on a 0.2 mmol scale. [b]nd = not determined. [c]Isolated yield after flash column chromatography on silica gel. [d]Determined with HPLC on a chiral stationary phase. [e]Ratio determined by ^1H NMR spectroscopy. [f]Obtained along with $(MePh_2Si)_2O$ (12%).

However, at shorter reaction times of 1 or 1.5 h, NMR spectroscopic analysis indeed showed substantial amounts of **22** (entries 2 and 3; see the Supporting Information for further details). Similar to the case for imine **14**, the enantiomeric excess of (*S*)-**21a** turned out to be independent of the reaction time. Other hydrosilanes such as $MePh_2SiH$ and Et_3SiH also resulted in the formation of silyl ethers (*S*)-**21b** and (*S*)-**21c**, respectively (entries 4 and 5). Again, the influence of the hydrosilane on enantioinduction was rather minor. The corresponding silyl ethers were not isolated in these cases.

With regard to the results previously obtained in the C═N and C═O hydrosilylation, the high yields of amine (*S*)-**15** and silyl ethers (*S*)-**21** were unexpected. For similar but achiral $[\mathbf{1}]^+[BAr^F{}_4]^-$ the dehydrogenative N–Si coupling to the corresponding N-silyl enamine **17** is the major reaction pathway,[10b] and (depending on the hydrosilane) almost exclusive formation of the silyl enol ether **22** by dehydrogenative O–Si coupling is observed.[10a] These results are usually obtained after short reaction times or with removal of dihydrogen gas.[31] In the present case, high yields of the amine **15** (after hydrolysis) and silyl ethers **21** are formed after prolonged reaction times in closed vessels: i.e., without release of dihydrogen from the reaction mixture. For both **14** and **20**, the intermediate formation of dehydrogenative coupling products, that is, silyl enamine **17** and silyl enol ether **22**, was verified. On this basis, a preliminary mechanistic picture can be formulated (Scheme 4): the preferred reaction pathway starts with hydrosilane activation by **I**, resulting in the formation of hydrosilane adduct **II** (**I** → **II**). The silyl unit of **II** is then transferred onto the Lewis basic nitrogen or oxygen atom of starting material **III**; this step leads to silyliminium or carboxonium ion **IV** (**II** + **III** → **IV** + **V**, gray box). On the basis of the results obtained for short reaction times, the catalytic cycle proceeds now with the deprotonation of **IV** by the Lewis basic sulfur atom of the neutral ruthenium hydride complex **V**. The C═C bond in **VII** is formed along with the dihydrogen adduct **VI** of the initial cationic complex (**IV** + **V** → **VI** + **VII**). This adduct is in equilibrium with free dihydrogen gas and the initial catalyst **I** (**VI** → **I** + H_2).[30] The backward reaction, i.e., dihydrogen activation with **I**,[1] eventually results in hydrogenation of the double bond in **VII**. Even though a

Scheme 4. Mechanism of the Net C═N and C═O Hydrosilylation

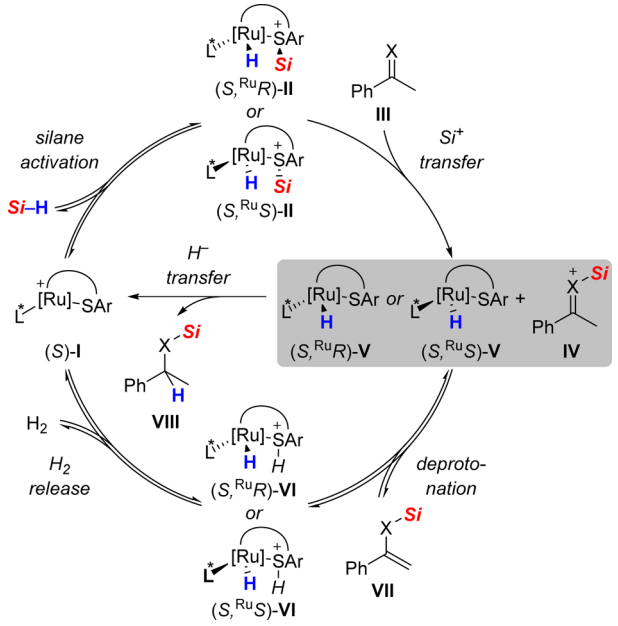

concerted mechanism is conceivable for this hydrogenation,[32] it is assumed to occur stepwise. It commences with proton transfer from **VI** to **VII** (**VI** + **VII** → **IV** + **V**). Hydride **V** then serves as a reducing agent for **IV**, resulting in the products **VIII**.

This two-step pathway is a dehydrogenative coupling–hydrogenation sequence resulting in net hydrosilylation of C═N and C═O groups. The sequence involves both cooperative Si–H and H–H bond activation. However, as the N-silyl enamine and the silyl enol ether **VII** have never been obtained *exclusively*, the direct hydrosilylation pathway is likely to compete to a certain extent; **VIII** is then directly obtained from **IV** through hydride transfer from **V**. Intermediates **V** and **IV** (gray box in Scheme 4) in the enantioselectivity-determining reduction step are *formally* the same for both scenarios: i.e., the direct reduction pathway and the enamine or enol reduction with dihydrogen. However, the enantiomeric excess obtained in the irreversible hydride transfer could still be significantly different for the following reason. The hydrosilane addition to **I** occurs *syn*[2] but with the chiral phosphine as ligand L* diastereomers ($S,^{Ru}R$)-**II** and ($S,^{Ru}S$)-**II** are obtained. These will *form* and *react* at different rates to yield diastereomeric ruthenium(II) hydrides ($S,^{Ru}S$)-**V** and ($S,^{Ru}R$)-**V**. **V** formed through dihydrogen activation with **I** and subsequent protonation of **VII** will most likely differ in the diastereomeric ratio. The more bulky silyl group (in comparison to the hydrogen atom) will likely allow for better differentiation of the diastereotopic sides in **I**.[33] The discrete diastereomeric ratios obtained for **V**, originating from either **II** or **VI**, will most probably lead to different enantiomeric excesses of **VIII**. Furthermore, the experimental data obtained with chiral catalyst $[(S)\text{-}\mathbf{13}]^+[BAr^F{}_4]^-$ allow for the exclusion of potential side-reaction pathways. Inconsistent ee values in the borane-catalyzed imine hydrosilylation had been investigated in great detail by us,[34] revealing a competing deprotonation of silyliminium ion **IV** (X = NR; Scheme 5, gray box) with unreacted starting material **III** (**III** + **IV** → **XI** + **VII**, clockwise pathway top left). The resulting iminium ion **IX** can also accept a hydride from **V** to form **X** with unknown enantioinduction (**V**

DOI: 10.1021/acs.organomet.7b00030
Organometallics XXXX, XXX, XXX–XXX

Scheme 5. Side Reactions in the Net C═N and C═O Hydrosilylation[a]

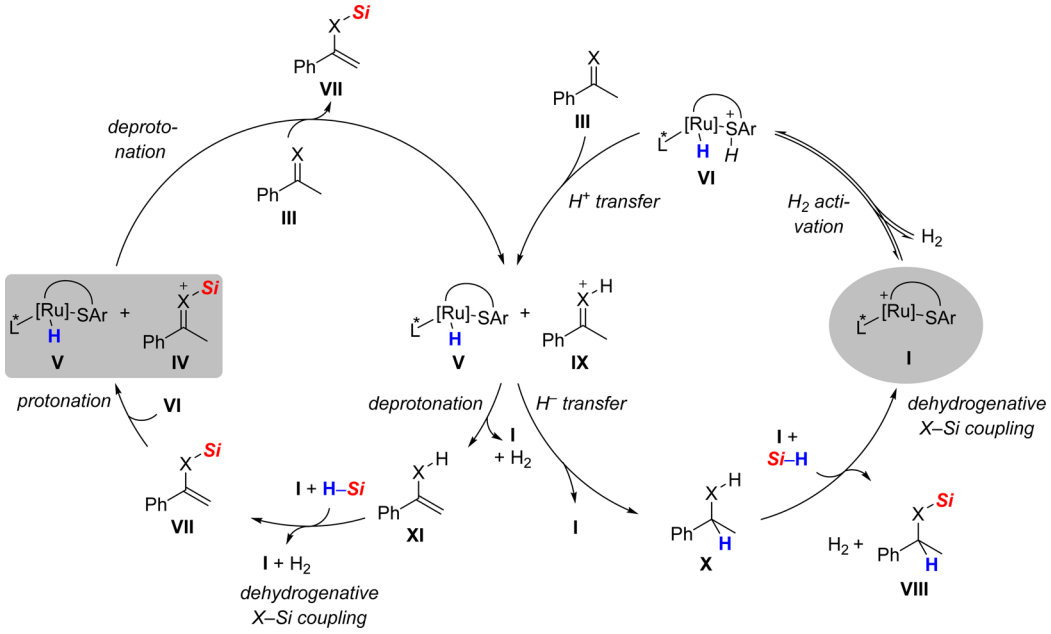

[a]For the sake of clarity, stereodescriptors have been omitted, and the diastereomers of **V** and **VI** are not shown.

+ **IX** → **X** + **I**, counterclockwise bottom right). **X** would undergo dehydrogenative N–Si or O–Si coupling[35] with **I** and hydrosilane to form **VIII** (**X** + **I** + *Si*–H → **VIII** + **I** + H_2). The global ee would hence be determined by the reduction of two different ions **IV** and **IX**. As **III** is consumed over the course of the reaction, the amount of **IX** decreases with increasing conversion and, consequently, the overall enantioselectivity would depend on the reaction time. Consistent ee values for both **14** and **20** were obtained in the reduction catalyzed by $[(S)\text{-}\mathbf{13}]^+[BAr^F{}_4]^-$, and this clearly excludes such a deprotonation–reduction sequence.

However, dihydrogen activation with **I** (Scheme 5, gray oval) and subsequent proton transfer of **VI** onto **III** also leads to **IX** (**VI** + **III** → **V** + **IX**, counterclockwise top right). In addition to the direct reduction with **V** (**IX** → **X** → **VIII**, counterclockwise bottom right), the formation of **XI** through deprotonation by **V** must be considered as another possibility (**V** + **IX** → **XI**, clockwise bottom left).[36] **XI** could then react in a dehydrogenative coupling to **VII** (**XI** + **I** + *Si*–H → **VII** + **I** + H_2). Protonation by dihydrogen adduct **VI** would then result in the two intermediates **V** and **IV** (**VII** + **VI** → **V** + **IV**). In principle, the formation of **V** and **IX** from **I** is possible as the hydrogenation of imines with $[\mathbf{1}]^+[BAr^F{}_4]^-$ was recently reported by us,[30] and the hydrogenation of **20** with $[\mathbf{1}]^+[BAr^F{}_4]^-$ is also known.[1] Transformations of hydrosilanes and catalysts $[\mathbf{1}]^+[BAr^F{}_4]^-$ are however generally more facile than those involving the splitting of dihydrogen. Hydrogenation reactions require pressures between 5.0 and 10 bar for full conversions of **III**.[37,38] The formation of **V** and **IX** is hence less favored compared to **V** and **IV**, and the following 3-step sequence (Scheme 5, clockwise bottom left) seems very unlikely. In addition, the direct reduction through hydride transfer from **V** onto **IX** (**V** + **IX** → **I** + **X**, Scheme 5, counterclockwise bottom right) and subsequent dehydrogenative N–Si and O–Si coupling (**X** + **I** + *Si*–H → **VIII** + **I** + H_2) can be largely dismissed because N-silyl enamines and silyl enol ethers are not formed by this pathway but are observed in substantial quantities. Furthermore, hydride transfer onto iminium or carboxonium ion **IX** is independent of the hydrosilane used in the net hydrosilylation. However, we did observe different levels of enantioinduction in reduction of **14** and **20** with different hydrosilanes (Tables 2 and 3)

CONCLUSION

We disclosed here an enantioselective net hydrosilylation of enolizable imines and ketones catalyzed by the chiral ruthenium complex $[(S)\text{-}\mathbf{13}]^+[BAr^F{}_4]^-$. These reductions are a rare example of asymmetric catalysis where just one chiral monodentate phosphine ligand at the transition metal is responsible for the enantioinduction. The obtained enantiomeric excesses are moderate, but this work still represents the first example of an enantioselective net C═X hydrosilylation involving cooperative Si–H bond activation. It also includes the first example of an enantioselective transfer hydrosilylation employing a hydrosilane surrogate. An experimental mechanistic analysis revealed that a two-step mechanism involving successive dehydrogenative X–Si coupling and enamine/enol ether hydrogenation is mainly operative. Both steps require bond activation at Ru–S bond of the catalyst, that is, Si–H bond activation in the first step and heterolytic H–H cleavage in the second step.

EXPERIMENTAL SECTION

General Remarks. All reactions were performed in flame-dried glassware using an MBraun glovebox (O_2 <10 ppm, H_2O <2 ppm) or conventional Schlenk techniques under a static pressure of argon (glovebox) or nitrogen. CH_2Cl_2, C_6H_6, and *n*-hexane were purified and dried using an MBraun solvent system. Toluene was distilled over sodium, degassed, and stored in the glovebox over 4 Å molecular sieves. CD_2Cl_2 and C_6D_6 were degassed and stored in a glovebox over 4 Å molecular sieves. $CDCl_3$ was stored over Cs_2CO_3. Technical grade solvents for extraction and chromatography (cyclohexane, CH_2Cl_2, ethyl acetate, and *tert*-butyl methyl ether) were distilled prior to use. (*S*)-2,2′-Dimethyl-1,1′-binaphthalene,[39] phosphine (*S*)-**6**,[40] phosphine (*S*)-**8**,[21] 2,6-dimesitylphenylthiole (HSdmp),[41] dichloro(*p*-cymene)-

DOI: 10.1021/acs.organomet.7b00030
Organometallics XXXX, XXX, XXX–XXX

ruthenium(II) dimer,[42] ruthenium complex **12**,[1] $NaBAr^F_4$,[43] imine **14**,[44] and surrogate **19**[29a] were synthesized according to reported procedures. TMEDA and dichlorophenylphosphine were distilled before use. Hydrosilanes and acetophenone (**20**) were degassed and stored in a glovebox over 4 Å molecular sieves. All other commercially available reagents were used as received. Analytical thin-layer chromatography (TLC) was performed on silica gel SIL G-25 glass plates from Macherey-Nagel. Flash column chromatography was performed on silica gel 60 (40−63 μm, 230−400 mesh, ASTM) by Merck using the indicated solvents. ^{1}H, ^{7}Li, ^{11}B, ^{13}C, ^{19}F, ^{29}Si, and ^{31}P NMR spectra were recorded in $CDCl_3$, C_6D_6, or CD_2Cl_2 on Bruker AV 400, Bruker AV 500, and Bruker AV 700 instruments. Chemical shifts are reported in parts per million (ppm) downfield from tetramethylsilane and are referenced to the residual solvent resonance as the internal standard ($CHCl_3$, δ 7.26 ppm for ^{1}H NMR; $CDCl_3$, δ 77.16 ppm for ^{13}C NMR; C_6D_5H, δ 7.16 ppm for ^{1}H NMR; C_6D_6, δ 128.06 ppm for ^{13}C NMR; $CHDCl_2$, δ 5.32 ppm for ^{1}H NMR; and CD_2Cl_2, δ 53.84 ppm for ^{13}C NMR). ^{7}Li, ^{11}B, ^{19}F, ^{29}Si, and ^{31}P NMR spectra were calibrated according to the IUPAC recommendation using a unified chemical shift scale based on the proton resonance of trimethylsilane as primary reference. Data are reported as follows: chemical shift, multiplicity (s_{br} = broad singlet, s = singlet, d = doublet, t = triplet, q = quartet, m = multiplet, m_c = centrosymmetric multiplet), coupling constant (Hz), integration. Signals labeled with asterisks overlapped with the residual solvent signal and were detected by 2D measurements (^{1}H,^{13}C HMQC, ^{1}H,^{13}C HSQC, and ^{1}H,^{13}C HMBC). High-resolution mass spectrometry (HRMS) and elemental analysis were performed by the Analytical Facility of the Institut für Chemie, Technische Universität Berlin. Infrared (IR) spectra were recorded on a Agilent Technologies Cary 630 FTIR spectrophotometer equipped with an ATR unit and are reported as wavenumbers (cm^{-1}). Melting points (mp) were determined with a Leica Galen III apparatus from Wagner & Munz and are not corrected. Enantiomeric excesses were determined by high-performance liquid chromatography (HPLC) analysis on an Agilent Technologies 1290 Infinity instrument with a chiral stationary phase using Daicel Chiralcel OJ-H or OD-H columns (*n*-heptane/isopropyl alcohol mixtures as solvent) or on an Agilent Technologies 1200 Infinity instrument with a stationary phase using a Daicel Chiralcel OJ-RH column (acetonitrile/water mixtures as solvent). Absolute configurations were assigned by comparison of the retention times of the enantiomers of **15**[44] and **21**[45] with literature data. Data for the single-crystal structure determination were collected with an Agilent SuperNova diffractometer equipped with a CCD area Atlas detector and a mirror monochromator by utilizing Cu Kα radiation (λ = 1.5418 Å). Software packages used: CrysAlis PRO for data collection, cell refinement, and data reduction,[46] SHELXS-97 for structure solution,[47] SHELXL-97 for structure refinement,[48] and Mercury 3.1.1[49] for graphics.

General Procedure for the Reduction of Imine 14 (GP1). Phenyl-protected imine **14** (39 mg, 0.20 mmol, 1.0 equiv) was added to a mixture of $NaBAr^F_4$ (1.8 mg, 2.0 μmol, 1.0 mol %) and the indicated ruthenium chloride complex (*R*,^{Ru}*RS*)-**9** (1.3 mg, 2.0 μmol, 1.0 mol %) or (*S*,^{Ru}*RS*)-**10** (1.7 mg, 2.0 μmol, 1.0 mol %) or to the preformed catalyst $[(S)\text{-}\mathbf{13}]^+[BAr^F_4]^-$ (3 mg, 2 μmol, 1 mol %) in a GLC vial. The indicated hydrosilane or surrogate (0.20 mmol, 1.0 equiv) and, in the case of Ph_3SiH, C_6H_6 (0.1 mL) were added. The mixture was stirred at room temperature for the indicated time, followed by the addition of cyclohexane (0.5 mL). Direct submission to flash column chromatography on silica gel (eluent cyclohexane/ethyl acetate 100/0 → 99/1) afforded amine (*S*)-**15** as a clear liquid.

General Procedure for the Reduction of Ketone 20 (GP2). Acetophenone (**20**; 24 mg, 0.20 mmol, 1.0 equiv) was placed in a GLC vial, and the ruthenium catalyst $[(S)\text{-}\mathbf{13}]^+[BAr^F_4]^-$ (3 mg, 2 μmol, 1 mol %) was added. The GLC vial was closed tightly, and the corresponding hydrosilane (0.20 mmol, 1.0 equiv) was rapidly added through the septum of the GLC cap with a gastight syringe. The mixture was stirred at room temperature for the indicated time, followed by the addition of cyclohexane (0.5 mL). The mixture was directly subjected to flash column chromatography on silica gel (eluent cyclohexane/*tert*-butyl methyl ether 100/0 → 20/1) to afford the corresponding silyl ether (*S*)-**21**.

Ruthenium Chloride Complex (*R*,^{Ru}*RS*)-9. 2,6-Dimesitylphenylthiole (67 mg, 0.19 mmol, 2.0 equiv) was placed in a 25 mL Schlenk flask, dissolved in THF (5 mL), and the resulting solution was cooled to 0 °C. *n*-BuLi (2 M in hexanes, 0.09 mL, 0.2 mmol, 2 equiv) was added, and the resulting mixture was stirred for 30 min at room temperature. The mixture was then added via syringe to a suspension of dichloro(*p*-cymene)ruthenium(II) dimer (60 mg, 0.097 mmol, 1.0 equiv) in THF (4 mL) at 0 °C. The resulting dark green suspension was stirred at room temperature for 1 h, the solvent was removed under reduced pressure, and toluene (7 mL) was added. The mixture was filtered over a Schlenk frit into a solution of phosphine (*S*)-**6** (35 mg, 0.19 mmol, 2.0 equiv) in toluene (4 mL). The reaction mixture was stirred at 65 °C for 21 h. The solvent was removed under reduced pressure, and the residue was subjected to flash column chromatography on silica gel (eluent cyclohexane/*tert*-butyl methyl ether 1/2). Ruthenium chloride complex (*R*,^{Ru}*RS*)-**9** (56 mg, 0.085 mmol, 45%, dr = 52:48) was obtained as a red-brown solid. Mp: 108−110 °C (cyclohexane/*tert*-butyl methyl ether). R_f = 0.24 (cyclohexane/*tert*-butyl methyl ether 3/2). IR (ATR): $\tilde{\nu}$ 2914 (m), 2861 (m), 2725 (w), 2332 (w), 2116 (w), 1610 (w), 1574 (w), 1434 (m), 1382 (m), 1282 (m), 1215 (w), 1175 (w), 1107 (m), 1037 (m), 893 (m), 848 (m), 789 (m), 739 (s), 695 (s) cm^{-1}. HRMS (ESI): calculated for $C_{35}H_{42}PRuS^+$ $[M - Cl]^+$, 627.1783; found, 627.1794. NMR spectroscopic data for the major diastereomer are as follows. ^{1}H NMR (500 MHz, C_6D_6): δ/ppm 0.49 (t, $^3J_{H,H}$ = 6.6 Hz, 3H), 0.68−0.82 (m, 3H), 1.17 (s, 3H), 0.89−0.97 (m, 1H), 1.42 (d, $^2J_{H,P}$ = 10.1 Hz, 3H), 1.44 (s, 3H), 1.97 (m_c, 1H), 2.12 (d, $^2J_{H,P}$ = 3.0 Hz, 3H), 2.26 (s, 3H), 2.36 (s, 3H), 2.43 (s, 3H), 2.40−2.49 (m, 1H), 3.99 (d, $J_{H,P}$ = 5.5 Hz, 1H), 5.14 (s, 1H), 6.77 (dd, $^3J_{H,H}$ = 6.9 Hz, $^4J_{H,H}$ = 1.7 Hz, 1H), 6.95 (t, $^3J_{H,H}$ = 6.9 Hz, 1H), 6.97−7.04 (m, 4H), 7.08 (m_c, 2H), 7.61 (m_c, 2H). ^{13}C{^{1}H} NMR (126 MHz, C_6D_6): δ/ppm 8.3 (d, $^1J_{C,P}$ = 34.4 Hz), 13.7 (s), 17.0 (s), 17.1 (s), 17.4 (s), 20.9 (s), 21.0 (s), 21.4 (s), 23.9 (d, $^3J_{C,P}$ = 10.7 Hz), 25.5 (d, $^2J_{C,P}$ = 19.5 Hz), 25.5 (d, $^1J_{C,P}$ = 30.9 Hz), 79.9 (s), 85.7 (s), 93.1 (s), 93.9 (d, $J_{C,P}$ = 11.4 Hz), 100.6 (d, $J_{C,P}$ = 5.4 Hz), 111.3 (s), 121.7 (s), 126.0 (s), 128.3 (m_c, 2C),* 128.4 (s),* 129.2 (2s), 129.5 (d, $^4J_{C,P}$ = 1.9 Hz), 130.7 (d, $^3J_{C,P}$ = 7.5 Hz, 2C), 135.4 (s), 136.3 (s), 136.6 (d, $^1J_{C,P}$ = 36.8 Hz), 136.8 (s), 137.3 (s), 138.4 (s), 142.8 (s), 159.4 (d, $J_{C,P}$ = 2.6 Hz). ^{31}P{^{1}H} NMR (202 MHz, C_6D_6): δ/ppm 12.6. Selected NMR spectroscopic data for the minor diastereomer are as follows. ^{1}H NMR (500 MHz, C_6D_6): δ/ppm 0.49 (t, $^3J_{H,H}$ = 6.6 Hz, 3H), 0.68−0.82 (m, 3H), 0.89 (s, 3H), 0.89−0.97 (m, 1H), 1.75 (d, $^2J_{H,P}$ = 10.1 Hz, 3H), 1.60 (s, 3H), 2.11 (d, $^2J_{H,P}$ = 3.2 Hz, 3H), 2.29 (s, 3H), 2.09−2.24 (m, 2H), 2.39 (s, 3H), 2.43 (s, 3H), 4.08 (d, $J_{H,P}$ = 5.2 Hz, 1H), 5.19 (s, 1H), 6.73 (dd, $^3J_{H,H}$ = 7.3 Hz, $^4J_{H,H}$ = 1.2 Hz, 1H), 6.82 (t, $^3J_{H,H}$ = 7.3 Hz, 1H), 6.97−7.04 (m, 4H), 7.08 (m_c, 2H), 7.54 (m_c, 2H). ^{13}C{^{1}H} NMR (126 MHz, C_6D_6): δ/ppm 9.4 (d, $^1J_{C,P}$ = 31.7 Hz), 13.7 (s), 16.5 (s), 17.3 (2s), 20.9 (s), 21.0 (s), 21.4 (s), 23.8 (d, $^3J_{C,P}$ = 11.5 Hz), 24.5 (d, $^1J_{C,P}$ = 32.5 Hz), 25.5 (d, $^2J_{C,P}$ = 19.5 Hz), 80.5 (s), 85.1 (s), 91.7 (s), 92.8 (d, $J_{C,P}$ = 11.0 Hz), 100.9 (d, $J_{C,P}$ = 5.6 Hz), 111.4 (s), 121.9 (s), 126.0 (s), 128.3 (m_c, 2C), 128.4 (s), 129.2 (2s), 129.4 (d, $^4J_{C,P}$ = 2.2 Hz), 130.7 (d, $^3J_{C,P}$ = 7.5 Hz, 2C), 135.4 (s), 136.3 (s), 136.6 (d, $^1J_{C,P}$ = 30.0 Hz), 136.8 (s), 137.4 (s), 138.5 (s), 142.8 (s), 159.4 (d, $J_{C,P}$ = 3.2 Hz). ^{31}P{^{1}H} NMR (202 MHz, C_6D_6): δ/ppm 13.4. Elemental analysis results were outside the tolerance range.

Ruthenium Chloride Complex (*S*,^{Ru}*RS*)-10. Phosphepine (*S*)-7 (0.12 g, 0.30 mmol, 1.0 equiv) was added to ruthenium complex **12** (0.19 mg, 0.30 mmol, 1.0 equiv), and the solids were dissolved in toluene (5 mL). The mixture was heated to 80 °C for 21 h. The solvent was removed under reduced pressure, and the resulting residue was directly subjected to flash column chromatography on silica gel (eluent: cyclohexane/*tert*-butyl methyl ether 3:2). Ruthenium chloride complex (*S*,^{Ru}*RS*)-**10** (0.18 g, 0.21 mmol, 71%, dr = 82:18) was obtained as a red-brown solid. Crystallization from a CH_2Cl_2/cyclohexane solution afforded single crystals from the major diastereomer suitable for X-ray analysis (see the Supporting Information for further details). Mp: 170−173 °C (cyclohexane/*tert*-butyl methyl ether). R_f = 0.2 (cyclohexane/*tert*-butyl methyl ether 3/

DOI: 10.1021/acs.organomet.7b00030
Organometallics XXXX, XXX, XXX−XXX

2). HRMS (ESI): calculated for $C_{52}H_{46}PRuS^+$ $[M - Cl]^+$, 835.2096, found, 835.2084. IR (ATR): $\tilde{\nu}$ 3046 (w), 2915 (m), 2847 (m), 2341 (w), 2114 (w), 1899 (w), 1718 (w), 1507 (m), 1432 (m), 1376 (m), 1250 (m), 1210 (m), 1104 (m), 1028 (m), 933 (m), 830 (s), 738 (s), 695 (s) cm^{-1}. NMR spectroscopic data for the major diastereomer (S,^{Ru}R)-**10** are as follows. ^{1}H NMR (500 MHz, CD_2Cl_2): δ/ppm 1.40 (s, 3H), 1.54 (s, 3H), 1.95 (s, 3H), 1.97 (s, 3H), 2.01 (d, $J_{H,P}$ = 3.6 Hz, 3H), 2.39 (s, 3H), 3.01 (dd, $^2J_{H,P}$ = 16.9 Hz, $^2J_{H,H}$ = 12.6 Hz, 1H), 3.38 (dd, $^2J_{H,H}$ = 14.8 Hz, $^2J_{H,P}$ = 3.6 Hz, 1H), 3.73 (dd, $^2J_{H,H}$ = 14.8 Hz, $^2J_{H,P}$ = 9.5 Hz, 1H), 4.30 (dd, $^2J_{H,H}$ = 12.6 Hz, $^2J_{H,P}$ = 2.9 Hz, 1H), 4.48 (d, $J_{H,P}$ = 5.1 Hz, 1H), 5.53 (s, 1H), 6.43 (s, 1H), 6.72 (dd, $^3J_{H,H}$ = 6.5 Hz, $^4J_{H,H}$ = 2.2 Hz, 1H), 6.90 (s, 1H), 6.90–6.93 (m, 2H), 6.96–6.97 (m, 2H), 7.08–7.11 (m, 1H), 7.17 (m_c, 1H), 7.32–7.35 (m, 3H), 7.39 (m_c, 2H), 7.48 (t, $^3J_{H,H}$ = 7.4 Hz, 1H), 7.62 (m_c, 2H), 7.65–7.66 (m, 1H), 7.73 (m_c, 2H), 7.77 (m_c, 1H), 7.86 (d, $^3J_{H,H}$ = 8.2 Hz, 1H). ^{13}C{^{1}H} NMR (126 MHz, CD_2Cl_2): δ/ppm 17.1 (s), 17.3 (s), 17.7 (s), 19.8 (s), 20.7 (s), 21.4 (s), 28.0 (d, $^1J_{C,P}$ = 25.0 Hz), 31.2 (d, $^1J_{C,P}$ = 24.7 Hz), 82.3 (s), 89.2 (s), 94.0 (s), 94.2 ($J_{C,P}$ = 11.3 Hz), 102.1 (d, $J_{C,P}$ = 6.2 Hz), 110.1 (s), 121.8 (s), 125.2 (s), 125.6 (s), 125.7 (s), 126.1 (s), 126.2 (s), 127.0 (s), 127.4 (s), 127.6 (s), 128.0 (s), 128.1 (s), 128.3 (s), 128.3 (s), 128.8 (d, $^3J_{C,P}$ = 8.4 Hz, 2C), 129.1 (d, $^3J_{C,P}$ = 1.8 Hz), 129.2 (s), 129.3 (s), 130.0 (s), 130.4 (s), 130.4 (d, $^2J_{C,P}$ = 6.7 Hz, 2C), 132.5 (s), 132.7 (d, $^2J_{C,P}$ = 6.7 Hz), 132.7 (2s), 132.9 (d, $^2J_{C,P}$ = 11.3 Hz), 133.3 (s), 133.7 (d, $^3J_{C,P}$ = 3.2 Hz), 134.7 (d, $^3J_{C,P}$ = 2.5 Hz), 135.7 (s), 136.0 (s), 136.2 (s), 136.5 (s), 137.7 (s), 138.5 (d, $^1J_{C,P}$ = 32.8 Hz), 142.2 (s), 157.7 (s). ^{31}P{^{1}H} NMR (202 MHz, CD_2Cl_2): δ/ppm 52.8. Selected NMR spectroscopic data for the minor diastereomer (S,^{Ru}R)-**10** are as follows. ^{1}H NMR (500 MHz, CD_2Cl_2): δ/ppm 1.06 (s, 3H), 1.81 (s, 3H), 2.05 (d, $J_{H,P}$ = 3.8 Hz, 1H), 2.08 (s, 3H), 2.14 (s, 3H), 2.30 (s, 3H), 3.06 (dd, $^2J_{H,P}$ = 16.9 Hz, $^2J_{H,H}$ = 12.9 Hz, 1H), 3.54 (dd, $^2J_{H,H}$ = 14.7 Hz, $^2J_{H,P}$ = 8.4 Hz, 1H), 3.63 (dd, $^2J_{H,H}$ = 14.7 Hz, $^2J_{H,P}$ = 3.5 Hz, 1H), 3.91 (dd, $^2J_{H,H}$ = 12.9 Hz, $^2J_{H,P}$ = 2.1 Hz, 1H), 4.87 (d, $J_{H,P}$ = 5.6 Hz, 1H), 5.28 (s, 1H), 6.88 (dd, $^3J_{H,H}$ = 7.0 Hz, $^4J_{H,H}$ = 1.5 Hz, 1H), 7.00 (t, $^3J_{H,H}$ = 7.0 Hz, 1H). ^{13}C{^{1}H} NMR (126 MHz, CD_2Cl_2): δ/ppm 16.4 (s), 17.1 (s), 17.6 (s), 20.6 (s), 20.9 (s), 21.3 (s), 30.6 (d, $^1J_{C,P}$ = 21.2 Hz), 31.6 (d, $^1J_{C,P}$ = 26.9 Hz), 80.9 (s), 85.2 (s), 93.4 (d, $J_{C,P}$ = 11.2 Hz), 94.9 (s), 100.3 (d, $J_{C,P}$ = 3.0 Hz), 115.0 (s), 121.9 (s), 126.1 (s), 128.1 (s), 128.2 (s), 129.0 (s), 136.0 (s), 136.1 (s), 136.5 (s), 136.7 (s), 138.0 (s), 142.0 (s), 158.4 (d, $^3J_{C,P}$ = 1.7 Hz). ^{31}P{^{1}H} NMR (202 MHz, C_6D_6): δ/ppm 51.2. Elemental analysis results were outside the tolerance range. The crystallographic data are available online in the CCDC database under number CCDC 1521692.

Cationic Ruthenium Complex [(*S*)-13]$^+$[BAr$^F_4$]$^-$. $NaBAr^F_4$ (0.10 g, 0.11 mmol, 1.0 equiv) was added to a solution of ruthenium chloride complex (*S*)-**10** (0.10 g, 0.11 mmol, 1.0 equiv) in CH_2Cl_2 (3 mL), and the mixture was stirred at room temperature for 3 h. The resulting green suspension was filtered over a PTFE syringe plug and rinsed with CH_2Cl_2 (3 × 2 mL). The solvent of the filtrate was evaporated under reduced pressure to afford the cationic ruthenium complex [(*S*)-**13**]$^+$[BAr^F_4]$^-$ (0.13 g, 77 μmol, 70%) as a green solid. HRMS (ESI): calculated for $C_{52}H_{46}PRuS^+$ $[M - BAr^F_4]^+$, 835.2096; found, 835.2103. ^{1}H NMR (500 MHz, C_6D_6): δ/ppm 1.05 (s, 3H), 1.20 (s, 3H), 1.35 (s, 3H), 1.74 (s, 3H), 1.99 (s, 3H), 1.99 (s, 3H), 2.43 (m_c, 1H), 2.52 (dd, $^2J_{H,H}$ = 14.3 Hz, $^2J_{H,P}$ = 4.3 Hz, 1H), 2.66 (d, $^2J_{H,H}$ = 12.6 Hz, 1H), 3.04 (dd, $^2J_{H,P}$ = 16.3 Hz, $^2J_{H,H}$ = 12.6 Hz, 1H), 3.50 (s, 1H), 3.96 (s, 1H), 6.42 (d, $^3J_{H,H}$ = 8.3 Hz, 1H), 6.52 (s, 1H), 6.70 (s, 1H), 6.77–6.80 (m, 3H), 6.94–7.00 (m, 5H), 7.04–7.06 (m, 1H), 7.10–7.15 (m, 2H), 7.18–7.26 (m, 4H), 7.36 (d, $^3J_{H,H}$ = 8.4 Hz, 1H), 7.52 (d, $^3J_{H,H}$ = 8.3 Hz, 1H), 7.55 (d, $^3J_{H,H}$ = 8.1 Hz, 1H), 7.65 (s_{br}, 4H), 7.69 (d, $^3J_{H,H}$ = 8.2 Hz, 1H), 8.38 (s_{br}, 8H). ^{13}C{^{1}H} NMR (126 MHz, C_6D_6): δ/ppm 17.4 (s), 17.7 (s), 18.0 (s), 20.2 (s), 20.5 (s), 21.0 (s), 31.5 (d, $^1J_{C,P}$ = 27.4 Hz), 33.0 (d, $^1J_{C,P}$ = 23.9 Hz), 73.5 (s), 73.6 (s), 103.1 (s), 105.0 (s), 105.5 (s), 107.9 (s), 118.1 (m_c, 4C), 125.3 (q, $^1J_{C,F}$ = 272 Hz, 8C), 126.6 (s), 126.7 (s), 126.7 (s), 127.1 (s), 127.1 (s), 127.1 (s), 127.2 (s), 127.9 (s), 128.0 (s), 128.3 (s), 128.5 (s), 128.6 (s), 128.6 (s), 128.7 (s), 128.8 (s), 128.9 (s), 129.3 (d, $^3J_{C,P}$ = 9.7 Hz, 2C), 129.9 (qq, $^2J_{C,F}$ = 31.2 Hz, $^4J_{C,F}$ = 2.8 Hz, 8C), 129.9 (s), 130.0 (s), 130.8 (d, $^1J_{C,P}$ = 35.7 Hz), 131.2 (d, $^2J_{C,P}$ = 10.7 Hz, 2C), 131.8 (s), 132.2 (s), 132.2 (s), 132.5 (d, $^4J_{C,P}$ = 2.1 Hz), 132.8 (s), 133.4 (s), 133.4 (s), 133.9 (s), 134.8 (s), 134.9 (s), 135.3 (s), 135.4 (s, 8C), 135.8 (s), 137.9 (s), 142.9 (s), 162.4 (m), 162.7 (q, $^1J_{C,B}$ = 49.9 Hz, 4C). ^{11}B{^{1}H} NMR (160 MHz, CD_2Cl_2): δ/ppm −6.6. ^{19}F{^{1}H} NMR (471 MHz, C_6D_6): δ/ppm −62.1. ^{31}P{^{1}H} NMR (203 MHz, C_6D_6): δ/ppm 40.4. Elemental analysis results were outside the tolerance range.

(*S*)-*N*-(1-Phenylethyl)aniline ((*S*)-15). Prepared according to GP1 from imine **14** (39 mg, 0.20 mmol, 1.0 equiv), catalyst [(*S*)-**13**]$^+$[BAr^F_4]$^-$ (3 mg, 2 μmol, 1 mol %), and Me_2PhSiH (40 μL, 0.20 mmol, 1.0 equiv). After it was stirred for 3 h at room temperature, the reaction mixture was directly subjected to flash column chromatography on silica gel (eluent cyclohexane/ethyl acetate 100/0 → 99/1). Amine (*S*)-**15** (38 mg, 0.19 mmol, 96%, 54% ee) was obtained as a clear liquid. HRMS (ESI): calculated for $C_{14}H_{16}N^+$ $[M + H]^+$, 198.1277; found, 198.1280. ^{1}H NMR (500 MHz, $CDCl_3$): δ/ppm 1.55 (d, $^3J_{H,H}$ = 6.7 Hz, 3H), 4.49 (q, $^3J_{H,H}$ = 6.7 Hz, 1H), 6.57 (d, $^3J_{H,H}$ = 8.1 Hz, 2H), 6.69 (m_c, 1H), 7.10 (m_c, 2H), 7.23 (tt, $^3J_{H,H}$ = 7.2 Hz, $^4J_{H,H}$ = 1.5 Hz, 1H), 7.32 (m_c, 2H), 7.36–7.39 (m, 2H), the NH signal was not detected. ^{13}C{^{1}H} NMR (126 MHz, $CDCl_3$): δ/ppm 24.7 (s), 54.4 (s), 114.2 (s, 2C), 118.2 (s), 126.2 (s, 2C), 127.2 (s), 128.8 (s, 2C), 129.2 (s, 2C), 144.6 (s), 146.4 (s). Elemental analysis results were outside the tolerance range. The enantiomeric excess was determined by HPLC analysis on a chiral stationary phase (Daicel Chiracel OD-H column, column temperature 20 °C, solvent *n*-heptane/isopropyl alcohol 90/10, flow rate 0.7 mL/min, λ 250 nm): t_R = 11.6 min for (*S*)-**15**, t_R = 14.4 min for (*R*)-**15**. If C_6D_6 (0.4 mL) is added to the reaction mixture after 0.5 h and the mixture is directly submitted to NMR spectroscopic analysis, the corresponding N-silyl enamine **17** is detected together with the N-silyl amine (*S*)-**16** (see the Supporting Information for a ^{1}H NMR spectrum). Selected NMR spectroscopic data for (*S*)-**16** (*Si* = $SiMe_2Ph$) are as follows. ^{1}H NMR (500 MHz, C_6D_6): δ/ppm 0.21 (s, 3H), 0.22 (s, 3H), 1.39 (d, $^3J_{H,H}$ = 7.0 Hz, 3H), 4.66 (q, $^3J_{H,H}$ = 7.0 Hz, 1H). Selected NMR spectroscopic data for **17** (*Si* = $SiMe_2Ph$) are as follows. ^{1}H NMR (500 MHz, C_6D_6): δ/ppm 0.33 (s, 3H), 0.35 (s, 3H), 5.07 (s, 1H), 5.45 (s, 1H). The analytical data for **15**,[44] **16**,[34] and **17**[34] are in accordance with those reported.

(*S*)-Dimethylphenyl(1-phenylethoxy)silane ((*S*)-21a). Prepared according to GP2 from acetophenone (**20**; 24 mg, 0.20 mmol, 1.0 equiv), catalyst [(*S*)-**13**]$^+$[BAr^F_4]$^-$ (3 mg, 2 μmol, 1 mol %), and Me_2PhSiH (31 μL, 0.20 mmol, 1.0 equiv). After 2 h at room temperature, the reaction mixture was directly subjected to flash column chromatography on silica gel (eluent cyclohexane/*tert*-butyl methyl ether 100/0 → 20/1). Silyl ether (*S*)-**21a** (48 mg, 0.19 mmol, 93%, 65% ee) was obtained as a clear liquid. HRMS (ESI): calculated for $C_{16}H_{19}OSi^+$ $[M - H]^+$, 255.1200; found, 255.1196. ^{1}H NMR (500 MHz, $CDCl_3$): δ/ppm 0.31 (s, 3H), 0.36 (s, 3H), 1.44 (d, $^3J_{H,H}$ = 6.4 Hz, 3H), 4.84 (q, $^3J_{H,H}$ = 6.4 Hz, 1H), 7.22–7.26 (m, 1H), 7.29–7.33 (m, 4H), 7.35–7.42 (m, 3H), 7.56–7.58 (m, 2H). ^{13}C{^{1}H} NMR (126 MHz, $CDCl_3$): δ/ppm −1.2 (s), − 0.7 (s), 27.0 (s), 71.2 (s), 125.6 (s, 2C), 127.0 (s), 127.9 (s, 2C), 128.3 (s, 2C), 129.7 (s), 133.7 (s, 2C), 138.3 (s), 146.4 (s). ^{29}Si{^{1}H} DEPT NMR (99 MHz, $CDCl_3$, optimized for J = 7 Hz): δ/ppm 6.6. Elemental analysis results were outside the tolerance range. The enantiomeric excess was determined by HPLC analysis on a chiral stationary phase (Daicel Chiracel OD-RH column, column temperature 20 °C, solvent acetonitrile/water 60/40, flow rate 0.3 mL/min, λ 210 nm): t_R = 35.2 min for (*S*)-**21a**, t_R = 37.5 min for (*R*)-**21a**. In cases of reaction times between 0.5 and 1.5 h, silyl ether **22** is obtained as a side product. Selected NMR spectroscopic data for **22** (*Si* = $SiMe_2Ph$) are as follows. ^{1}H NMR (500 MHz, $CDCl_3$): δ/ppm 0.55 (s, 6H), 4.35 (d, $^2J_{H,H}$ = 1.9 Hz, 1H), 4.87 (d, $^2J_{H,H}$ = 1.9 Hz, 1H). The analytical data for **21a**[45] and **22**[10a] are in accordance with those reported.

(*S*)-Methyldiphenyl(1-phenylethoxy)silane ((*S*)-21b). Prepared according to GP2 from acetophenone (**20**; 24 mg, 0.20 mmol, 1.0 equiv), catalyst [(*S*)-**13**]$^+$[BAr^F_4]$^-$ (3 mg, 2 μmol, 1 mol %), and $MePh_2SiH$ (40 μL, 0.20 mmol, 1.0 equiv). After 3 h at room temperature, the reaction mixture was directly subjected to flash column chromatography on silica gel (eluent cyclohexane/*tert*-butyl

DOI: 10.1021/acs.organomet.7b00030
Organometallics XXXX, XXX, XXX−XXX

methyl ether 100/0 → 20/1). Silyl ether (*S*)-**21b** (52 mg, 0.16 mmol, 82%, 66% ee) was obtained as a clear liquid along with small amounts of $(Ph_2MeSi)_2O$ (12%). HRMS (ESI): calculated for $C_{21}H_{21}OSi^+$ $[M - H]^+$, 317.1356; found, 317.1362. ^1H NMR (500 MHz, C_6D_6): δ/ppm 0.51 (s, 3H), 1.40 (d, $^3J_{H,H}$ = 6.4 Hz, 3H), 4.91 (q, $^3J_{H,H}$ = 6.4 Hz, 1H), 7.06 (tt, $^3J_{H,H}$ = 7.3 Hz, $^4J_{H,H}$ = 1.3 Hz, 1H), 7.13−7.19 (m, 8H), 7.28−7.30 (m, 2H), 7.60−7.66 (m, 4H). $^{13}C\{^1H\}$ NMR (126 MHz, $CDCl_3$): δ/ppm −2.2 (s), 27.2 (s), 72.0 (s), 125.0 (s), 127.3 (s), 128.2 (s, 2C),* 128.2 (s, 2C),* 128.2 (2C),* 130.0 (s), 130.1 (s), 134.8 (s, 2C), 134.9 (s, 2C), 136.9 (s), 137.0 (s), 146.6 (s). $^{29}Si\{^1H\}$ DEPT NMR (99 MHz, $CDCl_3$, optimized for J = 7 Hz): δ/ppm −3.9. Elemental analysis results were outside the tolerance range. The enantiomeric excess was determined by HPLC analysis on a chiral stationary phase (Daicel Chiracel OJ-RH column, column temperature 20 °C, solvent acetonitrile/water 70/30, flow rate 0.4 mL/min, λ 254 nm): t_R = 19.8 min for (*R*)-**21b**, t_R = 23.9 min for (*S*)-**21b**. The analytical data are in accordance with those reported.[45]

(*S*)-Triethyl(1-phenylethoxy)silane ((*S*)-21c). Prepared according to GP2 from acetophenone (**20**; 24 mg, 0.20 mmol, 1.0 equiv), catalyst $[(S)\text{-}\mathbf{13}]^+[BAr^F{}_4]^-$ (3 mg, 2 μmol, 1 mol %), and Et_3SiH (32 μL, 0.20 mmol, 1.0 equiv). After 3 h at room temperature, the reaction mixture was directly subjected to flash column chromatography on silica gel (eluent cyclohexane/*tert*-butyl methyl ether 100/0 → 20/1). Silyl ether (*S*)-**21c** (39 mg, 0.16 mmol, 82%, 50% ee) was obtained as a clear liquid. ^1H NMR (500 MHz, $CDCl_3$): δ/ppm 0.57 (m_c, 6H), 0.92 (t, $^3J_{H,H}$ = 7.9 Hz, 9H), 1.43 (d, $^3J_{H,H}$ = 6.4 Hz, 3H), 4.87 (q, $^3J_{H,H}$ = 6.4 Hz, 1H), 7.22 (m_c, 1H), 7.29−7.35 (m, 4H). $^{13}C\{^1H\}$ NMR (126 MHz, $CDCl_3$): δ/ppm 5.0 (s, 3C), 6.9 (s, 3C), 27.4 (s), 70.7 (s), 125.4 (s, 2C), 126.9 (s), 128.2 (s, 2C), 147.1 (s). $^{29}Si\{^1H\}$ DEPT NMR (99 MHz, $CDCl_3$, optimized for J = 7 Hz): δ/ppm 18.4. Elemental analysis results were outside the tolerance range. The enantiomeric excess was determined by HPLC analysis on a chiral stationary phase (Daicel Chiracel OD-RH column, column temperature 20 °C, solvent acetonitrile/water 70/30, flow rate 0.3 mL/min, λ 210 nm): t_R = 21.8 min for (*S*)-**21c**, t_R = 24.4 min for (*R*)-**21c**. The analytical data are in accordance with those reported.[45]

■ ASSOCIATED CONTENT

Supporting Information

The Supporting Information is available free of charge on the ACS Publications website at DOI: 10.1021/acs.organomet.7b00030.

NMR spectra of the compounds synthesized in this paper and crystallographic data (PDF)

Crystallographic data (CIF)

■ AUTHOR INFORMATION

Corresponding Author

*E-mail for M.O.: martin.oestreich@tu-berlin.de.

ORCID

Susanne Bähr: 0000-0001-5113-7646

Martin Oestreich: 0000-0002-1487-9218

Notes

The authors declare no competing financial interest.

■ ACKNOWLEDGMENTS

This research was supported in part by the Deutsche Forschungsgemeinschaft (Oe 249/10-1). S.B. thanks the Studienstiftung des deutschen Volkes for a predoctoral fellowship (2015−2017), and M.O. is indebted to the Einstein Foundation (Berlin) for an endowed professorship. Dr. Timo Stahl (TU Berlin) is acknowledged for preliminary mechanistic investigations, and we thank Dr. Elisabeth Irran (TU Berlin) for the X-ray analysis as well as Franz-Lukas Haut (FU Berlin) for experimental support.

■ REFERENCES

(1) Ohki, Y.; Takikawa, Y.; Sadohara, H.; Kesenheimer, C.; Engendahl, B.; Kapatina, E.; Tatsumi, K. *Chem. - Asian J.* **2008**, *3*, 1625−1635.

(2) Stahl, T.; Hrobárik, P.; Königs, C. D. F.; Ohki, Y.; Tatsumi, K.; Kemper, S.; Kaupp, M.; Klare, H. F. T.; Oestreich, M. *Chem. Sci.* **2015**, *6*, 4324−4334.

(3) For the first application of $[\mathbf{1}]^+[BAr^F{}_4]^-$ in catalytic Si−H bond activation, see: (a) Klare, H. F. T.; Oestreich, M.; Ito, J.-i.; Nishiyama, H.; Ohki, Y.; Tatsumi, K. *J. Am. Chem. Soc.* **2011**, *133*, 3312−3315. For a recent summary of electrophilic C−H silylation including the use of cationic ruthenium(II) complexes, see: (b) Bähr, S.; Oestreich, M. *Angew. Chem., Int. Ed.* **2017**, *56*, 52−59.

(4) Hydrodefluorination with $[\mathbf{1}]^+[BAr^F{}_4]^-$ (L = $(4\text{-}FC_6H_4)_3P$) is described in: Stahl, T.; Klare, H. F. T.; Oestreich, M. *J. Am. Chem. Soc.* **2013**, *135*, 1248−1251.

(5) The synthesis of dibenzosiloles with $[\mathbf{1}]^+[BAr^F{}_4]^-$ (L = $(4\text{-}FC_6H_4)_3P$) is reported in: (a) Omann, L.; Oestreich, M. *Angew. Chem., Int. Ed.* **2015**, *54*, 10276−10279. For the synthesis of indole-fused benzosiloles, see: (b) Omann, L.; Oestreich, M. *Organometallics* **2017**, *36*, 10.1021/acs.organomet.6b00801.

(6) The 1,4-hydrosilylation of pyridines is described in: Königs, C. D. F.; Klare, H. F. T.; Oestreich, M. *Angew. Chem., Int. Ed.* **2013**, *52*, 10076−10079.

(7) For the rhodium-catalyzed synthesis of chiral dibenzosiloles by cycloadditions, see: (a) Shintani, R.; Otomo, H.; Ota, K.; Hayashi, T. *J. Am. Chem. Soc.* **2012**, *134*, 7305−7308. (b) Shintani, R.; Takagi, C.; Ito, T.; Naito, M.; Nozaki, K. *Angew. Chem., Int. Ed.* **2015**, *54*, 1616−1620. For an example involving rhodium-catalyzed Si−C bond activation, see: (c) Onoe, M.; Baba, K.; Kim, Y.; Kita, Y.; Tobisu, M.; Chatani, N. *J. Am. Chem. Soc.* **2012**, *134*, 19477−19488. For a recent summary, see: (d) Shintani, R. *Asian J. Org. Chem.* **2015**, *4*, 510−514.

(8) Zaidlewicz, M.; Pakulski, M. M. In *Science of Synthesis Stereoselective Synthesis 2*; Molander, G. A., Ed.; Thieme: Stuttgart, 2011; pp 59−131.

(9) Xu, L.; Wu, X.; Xiao, J. In *Science of Synthesis Stereoselective Synthesis 2*; Molander, G. A., Ed.; Thieme: Stuttgart, 2011; pp 251−309.

(10) The dehydrogenative coupling as the major reaction pathway and minor hydrosilylation of ketones with $[\mathbf{1}]^+[BAr^F{}_4]^-$ (L = Et_3P) is reported in: (a) Königs, C. D. F.; Klare, H. F. T.; Ohki, Y.; Tatsumi, K.; Oestreich, M. *Org. Lett.* **2012**, *14*, 2842−2845. A similar transformation of imines is documented with $[\mathbf{1}]^+[BAr^F{}_4]^-$ (L = iPr_3P): (b) Hermeke, J.; Klare, H. F. T.; Oestreich, M. *Chem. - Eur. J.* **2014**, *20*, 9250−9254.

(11) For the synthesis and application of a cationic ruthenium(II) complex where the thiolate ligand and the η^6-mesityl ring are tethered by a chiral binaphthyl backbone, see: Wübbolt, S.; Maji, M. S.; Irran, E.; Oestreich, M. *Chem. - Eur. J.* **2017**, *23*, DOI: 10.1002/chem.201700304.

(12) Sterically demanding phosphines such as tBu_3P and 2-dicyclohexylphosphino-2′-methylbiphenyl (MePhos) or the electron-poor phosphine $(C_6F_5)_3P$ could not be applied to the synthesis of the catalyst precursors: Stahl, T. Ph.D. Thesis, Technische Universität Berlin, Berlin, Germany, 2014.

(13) For a review of the synthesis and application of monodentate chiral phosphines, see: (a) Lagasse, F.; Kagan, H. B. *Chem. Pharm. Bull.* **2000**, *48*, 315−324. (b) Hayashi, T. *Acc. Chem. Res.* **2000**, *33*, 354−362. Asymmetric hydrogenations are discussed in, for example: (c) Erre, G.; Enthaler, S.; Junge, K.; Gladiali, S.; Beller, M. *Coord. Chem. Rev.* **2008**, *252*, 471−491.

(14) (a) Knowles, W. S.; Sabacky, M. J. *Chem. Commun.* **1968**, 1445−1446. (b) Knowles, W. S.; Sabacky, M. J.; Vineyard, B. D. *J. Chem. Soc., Chem. Commun.* **1972**, 10−11.

(15) For the hydrosilylation of ketones with platinum complexes, see: Yamamoto, K.; Hayashi, T.; Kumada, M. *J. Organomet. Chem.* **1972**, *46*, C65−C67. For a summary, see also ref 13b.

DOI: 10.1021/acs.organomet.7b00030
Organometallics XXXX, XXX, XXX−XXX

(16) Several routes toward phosphorus-chiral phosphines have been documented: Grabulosa, A.; Granell, J.; Muller, G. *Coord. Chem. Rev.* **2007**, *251*, 25−90.
(17) The first asymmetric synthesis was accomplished by Gladiali: Gladiali, S.; Dore, A.; Fabbri, D.; de Lucchi, O.; Manassero, M. *Tetrahedron: Asymmetry* **1994**, *5*, 511−514.
(18) The derivatization and a potential application of **4** was later shown by Gladiali and Beller: (a) Junge, K.; Oehme, G.; Monsees, A.; Riermeier, T.; Dingerdissen, U.; Beller, M. *Tetrahedron Lett.* **2002**, *43*, 4977−4980. (b) Junge, K.; Hagemann, B.; Enthaler, S.; Spannenberg, A.; Michalik, M.; Oehme, G.; Monsees, A.; Riermeier, T.; Beller, M. *Tetrahedron: Asymmetry* **2004**, *15*, 2621−2631. For a summary, see: (c) Gladiali, S.; Alberico, E.; Junge, K.; Beller, M. *Chem. Soc. Rev.* **2011**, *40*, 3744−3763. See also ref 13c.
(19) For a copper-catalyzed enantioselective hydrosilylation of ketones with **4** as ligands, see: Junge, K.; Wendt, B.; Addis, D.; Zhou, S.; Das, S.; Beller, M. *Chem. - Eur. J.* **2010**, *16*, 68−73. For various applications including for example hydroboration or C−C bond formation reactions, see also ref 18c.
(20) The mechanism of the rhodium-catalyzed hydrosilylation with two phosphine ligands of type **3** on the rhodium center is presented in: Ojima, I.; Kogure, T.; Kumagai, M.; Horiuchi, S.; Sato, T. *J. Organomet. Chem.* **1976**, *122*, 83−97. For a detailed discussion and various examples of hydrogenations, see ref 13a. The use of a 2:1 ligand:metal ratio for the in situ generation of metal catalysts has also been established for **4**; see for example ref 19.
(21) Uozumi, Y.; Tanahashi, A.; Lee, S.-Y.; Hayashi, T. *J. Org. Chem.* **1993**, *58*, 1945−1949.
(22) Hayashi describes such a trend for a palladium-catalyzed hydrosilylation of double bonds: (a) Uozumi, Y.; Hayashi, T. *J. Am. Chem. Soc.* **1991**, *113*, 9887−9888. An allyl−monophosphine−palladium complex was later isolated during their studies of the reduction of allylic esters with formic acid: (b) Hayashi, T.; Iwamura, H.; Naito, M.; Matsumoto, Y.; Uozumi, Y.; Miki, M.; Yanagi, K. *J. Am. Chem. Soc.* **1994**, *116*, 775−776. For more examples employing **5** in asymmetric catalysis, see ref 13b.
(23) For a recent review of metal−ligand cooperation, see: Khusnutdinova, J. R.; Milstein, D. *Angew. Chem., Int. Ed.* **2015**, *54*, 12236−12273.
(24) (a) Jugé, S.; Genêt, J.-P. *Tetrahedron Lett.* **1989**, *30*, 2783−2786. (b) Jugé, S.; Stephan, M.; Laffitte, J. A.; Genêt, J.-P. *Tetrahedron Lett.* **1990**, *31*, 6357−6360.
(25) The phosphorus atom in (*S*)-**7** is not a chiral center, as it lies in the C_2 axis of the binaphthyl backbone. The generation of two diastereomers is explained by the formation of another chiral center at the ruthenium atom.
(26) As we did not notice a difference in the performance of in situ generated and isolated catalyst $[(S)\text{-}\mathbf{13}]^+[BAr^F{}_4]^-$, we did not expect an enhancement of the enantiomeric excess for $[\mathbf{1}]^+[BAr^F{}_4]^-$ with phosphine (*S*)-**6** as ligand. Its cationic congener was hence not isolated.
(27) For $[\mathbf{1}]^+[BAr^F{}_4]^-$ with L = $(4\text{-}FC_6H_4)_3P$, the intermediate $[Ru(Sdmp)L_2]^+$ was observed during the chloride abstraction.[12] If such a complex is obtained in the chloride abstraction from $(S,^{Ru}RS)$-**10**, it would unlikely be an active catalyst, as this would affect the enantiomeric excess in comparison to the use of isolated $[(S)\text{-}\mathbf{13}]^+[BAr^F{}_4]^-$. We hence conclude that a complex with two phosphine ligands at the ruthenium center either is not formed or is not catalytically active.
(28) Products of such a transformation were previously obtained in case of large protective groups at the nitrogen atom in substantial amounts.[10b]
(29) **19** was introduced for transfer hydrosilylations by our laboratory; see: (a) Simonneau, A.; Oestreich, M. *Angew. Chem., Int. Ed.* **2013**, *52*, 11905−11907. (b) Keess, S.; Simonneau, A.; Oestreich, M. *Organometallics* **2015**, *34*, 790−799. For a recent summary of transfer hydrosilylation, see: (c) Oestreich, M. *Angew. Chem., Int. Ed.* **2016**, *55*, 494−499.
(30) For the use of $[\mathbf{1}]^+[BAr^F{}_4]^-$ with L = Et_3P or $(4\text{-}FC_6H_4)_3P$ in imine reductions, see: Lefranc, A.; Qu, Z.-W.; Grimme, S.; Oestreich, M. *Chem. - Eur. J.* **2016**, *22*, 10009−10016.
(31) The reactions presented in this work are performed in closed, small vials after fast addition of the hydrosilanes through septa (see the Experimental Section for further details). Otherwise, dihydrogen gas is immediately released from the reaction mixture. Reactions with **20** were usually stopped after 5 min,[10a] whereas those with imines were performed in open vessels.[10b]
(32) The question of a two-step or one-step hydrogenation of the double bond remains open. In the related imine hydrogenation, hydride **V** and iminium ion **IX** do not exist as separated molecules,[30] which could also hold for **IV** and **V**. On the other hand, a two-step mechanism seems likely, in analogy to the corresponding hydrosilylation.
(33) An NMR spectroscopic analysis of the hydrosilane adducts **II** is in principle possible,[2,11] whereas the spectroscopic evidence for the dihydrogen adduct **VI** is elusive.[1,30] We are hence unable to either compare diastereoselectivities in the two activation scenarios or correlate the preferred formation of one diastereomer with the enantioselectivity obtained in the hydride transfer step.
(34) For an in-depth investigation of the borane-catalyzed hydrosilylation of imines, see: Hermeke, J.; Mewald, M.; Oestreich, M. *J. Am. Chem. Soc.* **2013**, *135*, 17537−17546.
(35) The dehydrogenative N−Si coupling with $[\mathbf{1}]^+[BAr^F{}_4]^-$ (L = Et_3P) has been documented: Königs, C. D. F.; Müller, M. F.; Aiguabella, N.; Klare, H. F. T.; Oestreich, M. *Chem. Commun.* **2013**, *49*, 1506−1508.
(36) This transformation was shown to be a possible pathway in the stepwise hydrogenation of *N*,*N*-dialkyl iminium ions with ruthenium hydrides: Guan, H.; Iimura, M.; Magee, M. P.; Norton, J. R.; Zhu, G. *J. Am. Chem. Soc.* **2005**, *127*, 7805−7814.
(37) DFT calculations also support that the formation of **II** is more favorable than the formation of **VI**. The relative free energies for **II**[2] and **VI**[30] differ significantly, with **II** being the more stable intermediate.
(38) The reduction of silyl enol ethers with $[\mathbf{1}]^+[BAr^F{}_4]^-$ (L = Et_3P) readily occurs with 1 atm of H_2.[12]
(39) Prepared by slightly modified procedures starting from (*S*)-binol: (a) Sengupta, S.; Leite, M.; Raslan, D. S.; Quesnelle, C.; Snieckus, V. *J. Org. Chem.* **1992**, *57*, 4066−4068. (b) Ooi, T.; Kameda, M.; Maruoka, K. *J. Am. Chem. Soc.* **2003**, *125*, 5139−5151.
(40) The BH_3-protected precursor for (*S*)-**6** was synthesized according to a procedure from Genet and Jugé.[24] Decomplexation was performed with DABCO as described for similar phosphines: Bayardon, J.; Bernard, J.; Rémond, E.; Rousselin, Y.; Malacea-Kabbara, R.; Jugé, S. *Org. Lett.* **2015**, *17*, 1216−1219.
(41) Ellison, J. J.; Ruhlandt-Senge, K.; Power, P. P. *Angew. Chem., Int. Ed. Engl.* **1994**, *33*, 1178−1180.
(42) Prepared according to a modified procedure from: Sun, Y.; Machala, M. L.; Castellano, F. N. *Inorg. Chim. Acta* **2010**, *363*, 283−287.
(43) Prepared according to a modified procedure from: Brookhart, M.; Grant, B.; Volpe, A. F., Jr. *Organometallics* **1992**, *11*, 3920−3922.
(44) Imamoto, T.; Iwadate, N.; Yoshida, K. *Org. Lett.* **2006**, *8*, 2289−2292.
(45) Mewald, M. Ph.D. Thesis, Westfälische Wilhelms-Universität Münster, Münster, Germany, 2012.
(46) *Agilent CrysAlis PRO*; Agilent Technologies, Yarnton, U.K., 2012
(47) Sheldrick, G. M. *Acta Crystallogr., Sect. A: Found. Crystallogr.* **1990**, *46*, 467−473.
(48) Sheldrick, G. M. *Acta Crystallogr., Sect. A: Found. Crystallogr.* **2008**, *64*, 112−122.
(49) Cambridge Crystallographic Data Centre: http://www.ccdc.cam.ac.uk/Solutions/CSDSystem/Pages/mercury.aspx.

DOI: 10.1021/acs.organomet.7b00030
Organometallics XXXX, XXX, XXX−XXX